



## Digital Binary Phase-shift Keyed Signal Detector

O. V. Chernoyarov<sup>a,b,c</sup>, L. A. Golpaiegani<sup>\*c</sup>, A. N. Glushkov<sup>d</sup>, V. P. Lintvinenko<sup>e</sup>, B. V. Matveev<sup>e</sup>

<sup>a</sup> International Laboratory of Statistics of Stochastic Processes and Quantitative Finance, National Research Tomsk State University, Tomsk, Russia

<sup>b</sup> Department of Higher Mathematics and System Analysis, Maikop State Technological University, Maikop, Russia

<sup>c</sup> Department of Electronics and Nanoelectronics, National Research University "MPEI", Moscow, Russia

<sup>d</sup> Department of Infocommunication Systems and Technologies, Voronezh Institute of the Ministry of Internal Affairs of the Russian Federation, Voronezh, Russia

<sup>e</sup> Department of Radio Engineering, Voronezh State Technical University, Voronezh, Russia

### PAPER INFO

#### Paper history:

Received 26 September 2018

Received in revised form 17 February 2019

Accepted 07 March 2019

#### Keywords:

Phase-shift Keying

Signal Detection

Fast Digital Processing

Noise Interference

Interference Immunity

### ABSTRACT

We have developed the effective algorithm for detecting digital binary phase-shift keyed signals. This algorithm requires a small number of arithmetic operations over the signal period. It can be relatively easy implemented based on the modern programmable logic devices. It also provides high interference immunity by identifying signal presence when signal-to-noise ratio is much less than its working value in the receiving path. The introduced detector has intrinsic frequency selectivity and allows us to form the estimate of the noise level to realize the adaptive determination of decision threshold. In order to get confirmation of the detector operability and performance, we suggest the expressions for false alarm and missing probabilities. In addition, we have examined, both theoretically and experimentally, the influence of the detector parameters on its characteristics.

doi: 10.5829/ije.2019.32.04a.08

## 1. INTRODUCTION

In a number of radio engineering applications, it is necessary to detect the binary phase-shift keyed (PSK) radio signals [1-6]. Analog PSK signal detectors are described in literature [7-9]. Their disadvantages are complexity of implementation of analog frequency multipliers and high-stable narrow-band frequency filters. Digital signal processing increases opportunities for designing both the effective signal detection algorithms and the corresponding electronics. However, applying the common approaches for digital detection involves a large number of arithmetic operations to deal with each of the received signal samples that implies the use of expensive high-speed hardware.

On the basis of the fast digital algorithm for coherent processing of narrow-band signals [10, 11], we now introduce the simple digital PSK signal detector that

requires a small number of arithmetic operations over the signal period and can be efficiently implemented by means of modern programmable logic devices [12, 13].

## 2. PHASE-SHIFT KEYED SIGNALS

In digital communication systems, the binary PSK and differential PSK signals are widely applied [5, 6]. The ideal binary PSK signal takes the form of following expression:

$$s(t) = S \cos[2\pi f_0 t + \psi(t) + \psi_0] \quad (1)$$

where the signal parameters are:  $S$  is the amplitude,  $f_0 = 1/T_0$  is the carrier frequency,  $T_0$  is the period,  $\psi(t) = \pi a(t)$  and  $\psi_0$  are the signal and constant initial phase components,  $a(t)$  is the information signal that is equal to 0 or 1 within the symbol duration  $T = N_0 T_0$ ,

\*Corresponding Author's Email: leila.golpaiegani@gmail.com (L. A. Golpaiegani)

and  $N_0$  is the number of carrier periods over the information symbol.

At the output of the narrowband transmission path, the signal remains the PSK one, however the change of its amplitude appears at the boundaries of the information packages. This effect is shown in Figure 1a under  $f_0 = 10$  MHz,  $N_0 = 32$ , while the signal spectrum has the form presented in Figure 1b,  $\Delta f_0 = f - f_0$ , its bandwidth is equal to 625 kHz and the path pass band  $\Delta f_s$  at the level of 3 dB is the same.

### 3. SIGNAL PROCESSING

What is peculiar about the binary PSK signal is that we have elimination of phase modulation while frequency is doubled. This phenomenon, with the subsequent frequency division, is applied in phase lockers implemented according to Pistolkors' circuit [14].

To detect the PSK signal, it is necessary to arrange the frequency multiplication only, with the subsequent narrow-band filtration and estimation of the signal level at the frequency  $2f_0$ . Thus, the useful component is extracted and the estimate of the interference level is made by rejector filtration, which leads to the decision formed concerning either presence or absence of the input PSK signal. Such processing procedure is used in analog PSK signal detectors [7-9].

### 4. DIGITAL PSK SIGNAL DETECTOR

The block diagram of the fast digital binary PSK signal detector is presented in Figure 2. The input PSK signal is passed to the analog-to-digital converter (ADC). The ADC sampling rate  $f_Q$  is determined by clock generator (CG) and is equal to:

$$f_Q = 8f_0 \tag{2}$$

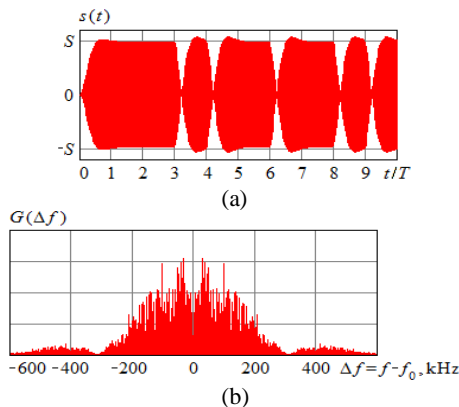


Figure 1. PSK signal and its spectrum

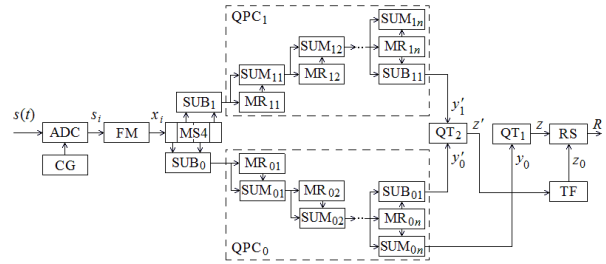


Figure 2. Digital PSK signal detector

The samples  $s_i$  are fed from the ADC output to the frequency multiplier (FM) at the times  $t_i$ , where  $i$  is the number of the sample. The digital multiplier (DM) presented in Figure 3a can be used as FM, and then the DM output sample  $x_i$  is equal to the square of the input sample. For ideal PSK signal (1), we get

$$x_i = s_i^2 = S^2 \cos^2[2\pi f_0 t_i + \psi(t) + \psi_0] = 0.5S^2 + 0.5S^2 \cos(4\pi f_0 t_i + 2\psi_0) \tag{3}$$

Thus, the high-frequency response of the multiplier is the harmonic oscillation with the frequency  $2f_0$  which does not depend on the modulating signal. For actual PSK signals, the FM response will be much more narrow-band than the input signal.

In order to double the frequency (to form the second harmonic of the input signal), we can use simpler, but less effective input sample module operation (Figure 3b):

$$x_i = |s_i| = |S \cos[2\pi f_0 t_i + \psi(t) + \psi_0]| \tag{4}$$

However, in this case, other unwanted high-frequency harmonics happen to be present in the spectrum of the FM response. Therefore, further, we are to use the quadratic transformation (3) for doubling the signal frequency.

In Figure 4a, we can see the signal spectrum at the FM output in the neighborhood of the double frequency  $2f_0$ , while the interferences are absent and the input signal takes the form presented in Figure 1. In Figure 4b, the segment of this spectrum is selected close to the point  $2f_0$ . Here

$$\Delta f = f - 2f_0 \tag{5}$$

is the frequency detuning. As it follows from Figure 4, the FM output signal is a very narrow-band one.



Figure 3. Possible schemes for implementation of frequency multiplier

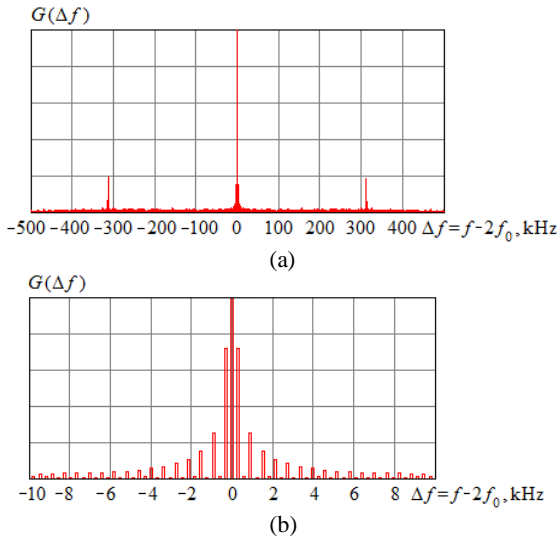


**Figure 4.** The signal spectrum at the output of the frequency multiplier

In  $SUM_{01}$  that is a summator of  $QPC_0$  unit, the difference  $(x_0 - x_2)$  is added to the very same difference but calculated at the previous period of the second harmonic and thus saved earlier into the multibit one cell shifter  $MR_{01}$ . Further, in  $SUM_{02}$ , the obtained sum of the adjacent differences  $(x_0 - x_2)$  is added to the value from the multibit three cell shifter  $MR_{02}$  calculated earlier for the previous pair of periods. As a result, at the output of the  $SUM_{0n}$  summator, we get

$$y_{0i} = \sum_{k=0}^{N-1} (x_{0i-k} - x_{2i-k}) \tag{6}$$

Here  $n = \log_2 N$ ,  $N$  is the number of the second harmonic periods through which the averaging of the even samples differences is carried out and  $i$  is the number of the current period of the PSK signal second harmonic.

The  $QPC_1$  unit operates likewise and at the output of the  $SUM_{1n}$  summator we obtain the accumulated sum

$$y_{1i} = \sum_{k=0}^{N-1} (x_{1i-k} - x_{3i-k}) \tag{7}$$

The samples differences in the quadrature channels are time shifted by the quarter-period of the second harmonic (equivalent to the phase shift by  $90^\circ$ ). Then, it is easy to show that for the ideal PSK signal the value

$$z_i = \sqrt{y_{0i}^2 + y_{1i}^2} \tag{8}$$

at the output of the quadratic block  $QT_1$  is constant and equal to

$$z_i = 2NS_2 \tag{9}$$

Here  $S_2$  is the amplitude of the input signal second harmonic which is equal to  $0.5S^2$  while applying the quadratic transformation (3).

In order to estimate the interference level at the reception path, it is necessary to suppress the signal central frequency at the FM output (Figure 3b) and to extract the remaining frequency components. For this purpose, by means of the  $SUB_{01}$  and  $SUB_{11}$  subtractors, the values

$$y'_{0i} = \sum_{k=0}^{N/2-1} (x_{0i-k} - x_{2i-k}) - \sum_{k=N/2}^{N-1} (x_{0i-k} - x_{2i-k}) \tag{10}$$

$$y'_{1i} = \sum_{k=0}^{N/2-1} (x_{1i-k} - x_{3i-k}) - \sum_{k=N/2}^{N-1} (x_{1i-k} - x_{3i-k})$$

are formed and on that basis the response at the output of the quadratic block  $QT_2$

$$z'_i = \sqrt{y_{0i}'^2 + y_{1i}'^2} \tag{11}$$

is generated. With the help of Equation (11), the threshold  $z_0$  is calculated by averaging the responses of the interference estimate channel over  $M_0 = 2^m$  samples with the weighting coefficient  $\alpha$ :

$$z_{0i} = \alpha \sum_{k=0}^{M_0-1} z'_{i-Nk} \tag{12}$$

The adjacent samples  $z'_i$  are strongly correlated. Therefore, it is practical to carry out their averaging in the following way, for example:

$$z_{0i} = \alpha \sum_{k=0}^{M_0-1} z'_{i-Nk} \tag{13}$$

This would require applying significantly lower values of  $M_0$  and  $m$ . The block diagram of the threshold former TF is shown in Figure 5.

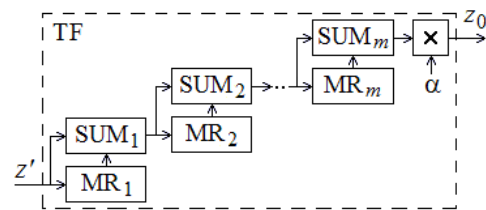


**Figure 5.** The threshold former

The value  $z_{0i}$  of threshold incomes into the resolver RS and if

$$z_i > z_{0i} \tag{14}$$

then the decision  $R$  is made that the binary PSK signal is present, otherwise – that it is absent.

The transformations (7) and (11) conform with the classical non-coherent signal processing procedure [5, 6]. In the practical implementation of the detector, we can omit the square-rooting operation and use the decision statistics of the form of  $z_i = y_{0i}^2 + y_{1i}^2$ ,  $z'_i = y'_{0i}{}^2 + y'_{1i}{}^2$ .

### 5. THE FREQUENCY CHARACTERISTICS OF THE SIGNAL AND NOISE PROCESSING CHANNELS

In terms of z-transform [15], the detector transfer function for the signal extraction channel (by the response  $z$ ) can be presented as follows:

$$H(z) = (1 - z^{-2})(1 + z^{-4}) \times (1 + z^{-8}) \dots (1 + z^{-N})(1 + z^{-2N}) \tag{15}$$

and for the interference estimate channel (by the response  $z$ ) – as follows:

$$H'(z) = (1 - z^{-2})(1 + z^{-4}) \times (1 + z^{-8}) \dots (1 + z^{-N})(1 - z^{-2N}) \tag{16}$$

By substituting

$$z = \exp(j\pi f T_0 / 4) = \exp[j\pi(2f_0 + \Delta f) / 4f_0] \tag{17}$$

into Equations (15), (16), where  $j = \sqrt{-1}$  and  $f$  is the signal frequency at the FM output. We obtain the dependences of the frequency characteristics of the signal extraction and the interference estimate channel on the  $\Delta f$  detuning (5), that are  $H(\Delta f) = |H(z)|$  and  $H'(\Delta f) = |H'(z)|$ , respectively. These characteristics are in fact the ratios of the output response to the input signal amplitude at the frequency  $f$ . The graphs of the frequency characteristics  $H(\Delta f)$  and  $H'(\Delta f)$  are shown in Figure 6 by solid and dashed lines, correspondingly. We can see that there are provided both the extraction of the signal component and its cancellation in the interference estimate channel. As both signal processing channels are the narrow-band ones, the interference component is estimated within the signal frequency band (Figure 1b).

The maximum of the frequency characteristic of the signal extraction channel is equal to  $2N$ , while its nearest zeros hold under the detuning  $F = \pm 2f_0 / N$ .

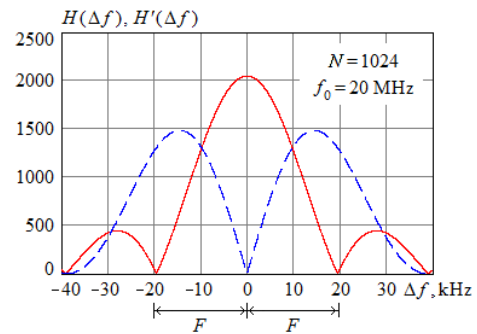


Figure 6. The frequency characteristics of the signal extraction channel and the interference estimate channel

The frequency characteristic of the interference estimate channel, in turn, becomes zero at the signal frequency  $f = 2f_0$ , and the cancellation is provided of the basic signal frequency components. Thus, the introduced PSK signal detector with the frequency characteristics of the form presented in Figure 6 allows extracting the useful signal as well as estimating the interference level when receiving the signal with the spectrum shown in Figure 4.

### 6. THE DETECTOR SIMULATION

The results of simulation of the digital detector are shown in Figures 7-9. In Figure 7, the normalized responses  $z/N$  (solid line) and  $z'/N$  (dashed line) are shown of the signal extraction channel and the interference estimate channel depending on the number  $k$  of the received information symbol under the unit signal amplitude  $S=1$  and in the absence of interferences. Figure 7a corresponds to the case of the ideal PSK signal (1) and Figure 7b – to the signal passing through the narrow-band reception path (Figure 1). The oscillations of the response  $z/N$  seen in Figure 7b are caused by the phase-shift keying occurring in the narrow-band reception path, while the oscillations of the response  $z'/N$  of the interference estimate channel are practically absent. At the start of the detection, when  $k < N_0$ , the transient process appears specified by the multibit shifters fill.

In the presence of interferences, their level can be estimated by the signal-to-noise ratio (SNR) at the output of the reception path as the ratio of the PSK signal power to the interference mean power (dispersion)  $\sigma_{in}^2$ :

$$h^2 = S^2 / 2\sigma_{in}^2 \tag{18}$$

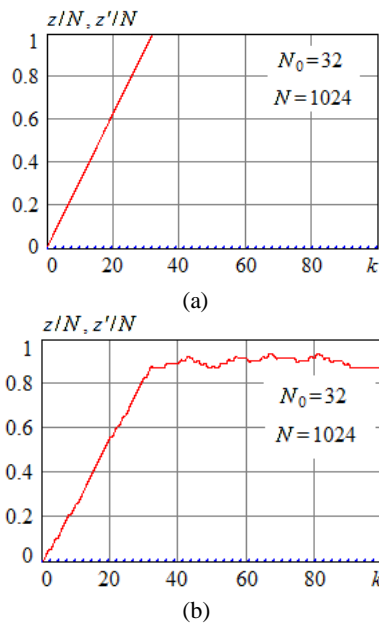


**Figure 7.** The normalized responses of the signal extraction channel and the interference estimate channel in the absence of interferences

In Figure 8, there are present the simulated results of the normalized responses  $z/N$  (solid line) and  $z'/N$  (dashed line) for a varied number of the averaging periods  $N$  of the input signal second harmonic and for different values of SNRs  $h$  at the output of the reception path. It is presupposed that  $f_0 = 10$  MHz,  $N_0 = 32$  and the PSK signal is distorted by Gaussian white noise passed through the narrow-band reception path with the bandwidth 625 kHz.

As it follows from Figure 8, under  $N = 2^{10} = 1024$  (i.e., when applying  $n = 10$  stages of the samples accumulation in Figure 2), the consistent signal detection is provided under  $h = 11$  dB (Figure 8a), while the interference immunity is greatly reduced under  $h \leq 5$  dB.

In this case, in order to decrease the error probability, the number of the averaging periods  $N$  should be increased. Thus, when  $h = 5$  dB, the interference immunity becomes high under  $N = 2^{12} = 4096$  or  $n = 12$  (Figure 8c). Under  $N = 2^{13} = 8192$  ( $n = 13$ ), the detector is operable even under  $h = -3$  dB (Figure 8d).

In Figure 9, there are drawn the dependences of the normalized detector response time in signal absence (“noise”) and in signal presence (“signal+noise”) under  $h = 5$  dB and various  $N$ . Here solid line corresponds to the signal channel, while dashed line – to the noise channel.

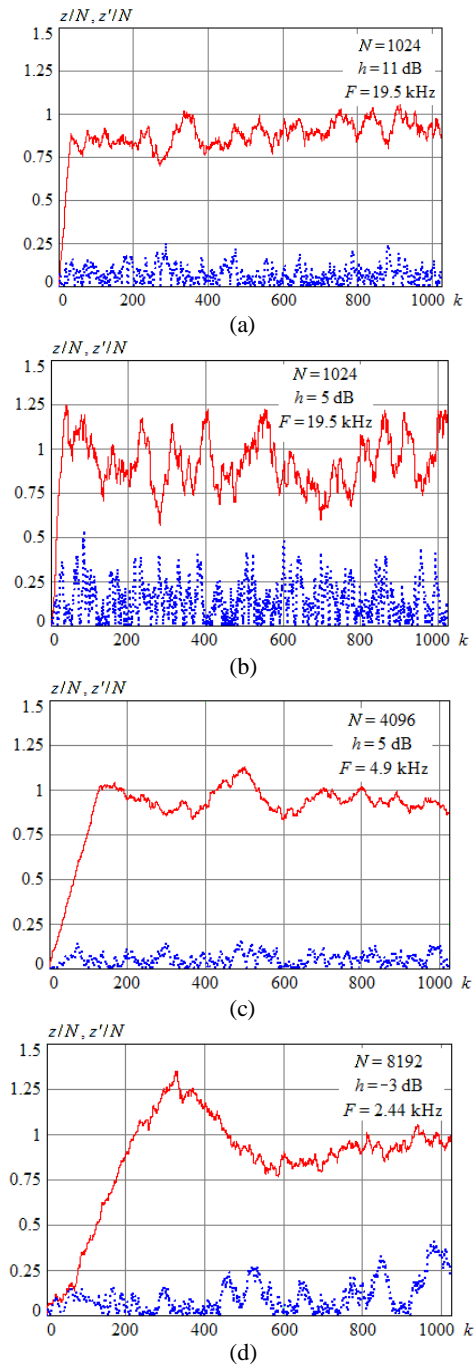


**Figure 8.** The normalized responses of the signal extraction channel and the interference estimate channel in the presence of the noise

As we can see, when the PSK signal is absent, in signal extraction channel and in interference estimate channel there are observed the interferences of the same intensity that decreases with  $N$  increasing. In the presence of the signal, the interference intensity increases in the interference estimate channel due to the incomplete signal cancellation.

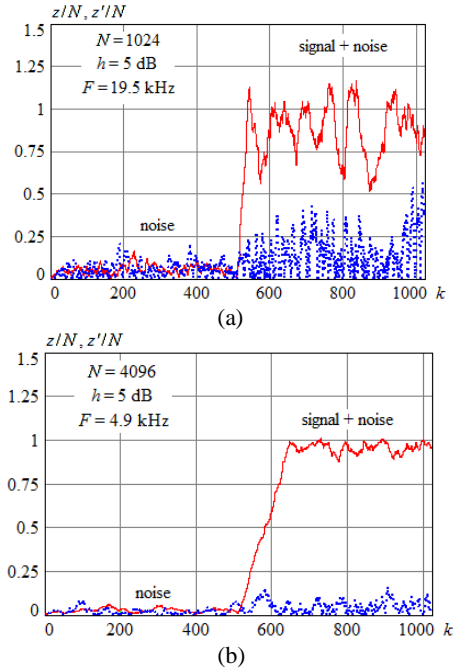


**Figure 9.** The normalized responses of the signal extraction channel and the interference estimate channel in the presence and in the absence of the signal

It should be noted that if non-Gaussian noise is present at the detector input, then at the outputs of the quadrature processing channels the values of the sums (6), (7) and (10) will obey Gaussian probability distribution under  $N \gg 1$ , according to the central limit theorem.

### 7. THE DETECTOR INTERFERENCE IMMUNITY

Now we will carry out a rough estimate of the interference immunity of the binary PSK signal detector. Let the band Gaussian noise with zero mean value and dispersion  $\sigma_{in}^2$  is present at the output of the narrow-band reception path with pass band  $\Delta f_s$  equal to the input PSK signal (1) spectrum width, while SNR  $h^2$  is determined by Equation (18).

In the signal absence, after passing the quadratic block, the noise has the mean value  $\sigma_{in}^2$  and dispersion  $2\sigma_{in}^4$  [16]. In the signal presence, considering the frequency range in the neighborhood of the frequency  $2f_0$ , at the output of the quadratic block, the mix of the harmonic wave with the amplitude  $s^2/2$  and the correlated noise process with the mean value  $\sigma_{in}^2$  and the dispersion  $2\sigma_{in}^4$  occurs.

In the quadrature processing channels, the summation or subtraction is implemented of  $N$  differences (6), (7) or (10) of the input samples with subsequent transformations (8) and (11) by the quadratic blocks  $QT_1$  and  $QT_2$ . As a result, according to literature [16], the response  $z$  of the signal extraction channel is described by Rice distribution with the probability density of the form

$$w_s(z) = \frac{z}{\sigma^2} \exp\left(-\frac{z^2 + a^2}{2\sigma^2}\right) I_0\left(\frac{az}{\sigma^2}\right) \quad (19)$$

where  $a = \sqrt{a_1^2 + a_2^2}$ ,  $a_1, a_2$  are the mean values and  $\sigma^2$  are the dispersions of the responses of the quadrature processing channels,  $I_0(x)$  is the zero-order modified Bessel function.

In the interference estimate channel, due to the subtractions in  $SUB_0$  and  $SUB_1$ , we get  $a=0$  and, as it follows from Equation (19), the response  $z'$  is described by Rayleigh probability density

$$w_n(z') = z' \exp(-z'^2/2\sigma^2) / \sigma^2 \quad (20)$$

The dispersions of the responses  $z$  and  $z'$  are the same and they are equal to

$$\sigma^2 = 4\sigma_{in}^4 \sum_{i=1}^N \sum_{k=1}^N R_{ik} \quad (21)$$

where  $R_{ik} = R(|i-k|\tau)$  is the correlation coefficient between  $i$ -th and  $k$ -th samples,  $R(\tau)$  is the normalized correlation function of the input noise,  $\tau = T_2/4$ ,  $T_2 = T_0/2$  are the second harmonic sampling interval and period. We designate  $\mu = \sum_{i=1}^N \sum_{k=1}^N R_{ik}$  and rewrite

Equation (21) as follows:

$$\sigma^2 = 4\sigma_{in}^4 \mu \quad (22)$$

If the samples can be considered as uncorrelated, i.e.

$$R_{ik} = \begin{cases} 1, & i = k, \\ 0, & i \neq k, \end{cases} \text{ then the formula (22) takes the form of}$$

$$\sigma^2 = 4N\sigma_{in}^4 \quad (23)$$

For the narrow-band Gaussian noise at the detector input resulting from, for example, the impact of Gaussian white noise on the high-Q oscillation circuit with the pass band  $\Delta f_c$ , we get [16]

$$R(\tau) = \exp(-\pi\Delta f_c \tau/2) \quad (24)$$

Assuming that in Equation (24)  $\tau = T_0/8$ , for the correlation coefficient values (21) we obtain

$$R_{ik} = \exp(-\pi\Delta f_c T_0|i-k|/16) \tag{25}$$

The product

$$\eta = \Delta f_c T_0 \tag{26}$$

characterizes the measure of input signal bandlimitedness. Taking into account the designation (26), we rewrite Equation (25) as follows

$$R_{ik} = \exp(-\pi\eta|i-k|/16) \tag{27}$$

In Figure 10a, by dashed line the dependence  $R_n$  (27) of the correlation coefficient is plotted as the function of the samples bias  $n = |i-k|$  under  $\eta = 0.0625$ ; while by solid line the corresponding dependence is drawn obtained by the statistical simulation for  $N = 1024$  and when processing the signal presented in Figure 1a. As we can see here, the considered theoretical and experimental models have agreed with each other satisfactorily. In Figure 10b, there is shown the dependence  $\mu(\eta)/N$  obtained under  $N = 1024$ . When  $\eta$  (26) is decreasing, the dispersions of the responses of the quadrature channels increase significantly. Thus, if  $\eta = 0.0625$  and  $N = 1024$ , then we get  $N \ll \mu = 3.95 \cdot 10^5 < N^2$ .

By applying Equation (20), we can write down the expression for the false alarm probability:

$$P_F = \int_{z_0}^{\infty} w_n(z) dz = \exp\left(-\frac{z_0^2}{2\sigma^2}\right) \tag{28}$$

Here  $z_0$  is the threshold with which the decision statistics (8) is compared. Specifying the false alarm probability (when the Neumann-Pirson criterion is used, for example), from Equation (28), makes it possible for us to calculate the values of the normalized threshold  $z_N = z_0/\sigma$  in the following way:

$$z_N = \sqrt{-2\ln P_F} \tag{29}$$

The dependence (29) is illustrated in Figure 11.

If the PSK signal is present at the detector input, then the decision statistics is described by Rice distribution (19) with the deviation parameter  $a = NS^2$  and the dispersion (23). Then, for the missing probability, we get:

$$P_M = \int_0^{z_0} w_s(z) dz = \int_0^{z_0} x \exp\left(-\frac{x^2 + N^2 h^4/\mu}{2}\right) I_0\left(\frac{N}{\sqrt{\mu}} h^2 x\right) dx \tag{30}$$

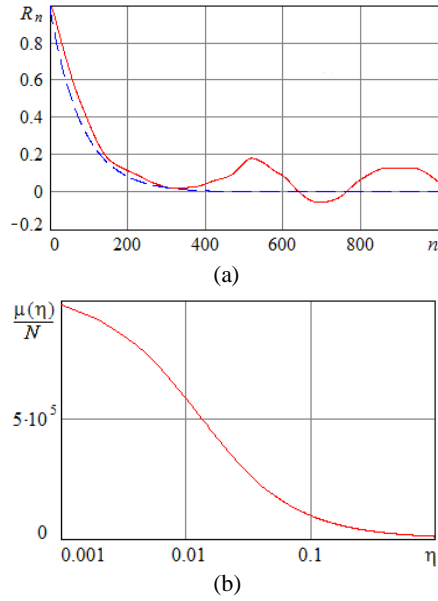


**Figure 10.** The correlation coefficient of the narrow-band Gaussian noise at the detector input and the normalized values of the parameter  $\mu$

In Figure 12, the dependences are shown of the false alarm (dashed line) and the missing (solid lines) probabilities on the normalized threshold  $z_N$  (29). It is assumed that  $N = 1024$  (Figure 12a) or  $N = 8192$  (Figure 12b) and SNR  $h$  (18) may vary: its values are 3, 4.8, 7 dB (Figure 12a), or -3, 0, 3 dB (Figure 12b).

It should be noted that the obtained approximate estimates of the error probabilities (28) and (30) do not account for increasing response of the interference estimate channel while the PSK signal occurs. This effect is caused by the imperfect signal cancellation that we can see in Figure 9.

Besides, while obtaining the formulas (28), (30), the correlation properties of the input signal are approximately taken into account. However, as it is demonstrated during the statistical simulation, in this case too the expressions (28), (30) for the error probabilities coincide satisfactorily with the corresponding experimental data.

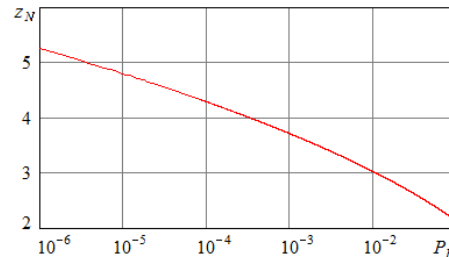


**Figure 11.** The correlation coefficient of the narrow-band Gaussian noise at the detector input and the normalized values of the parameter  $\mu$

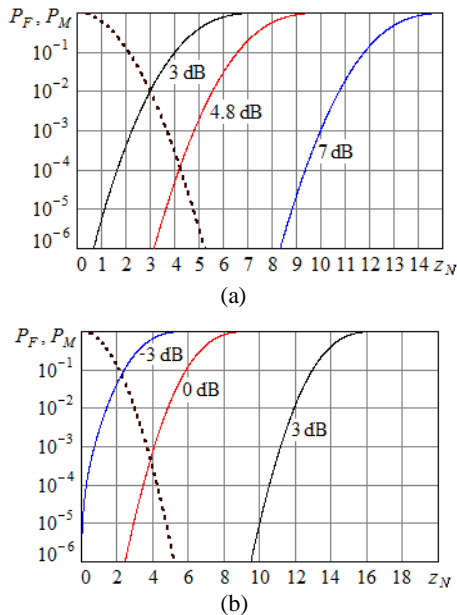


**Figure 12.** The false alarm and the missing probabilities under  $N=1024$  and  $N=8192$

Thus, the introduced algorithm for detecting the binary PSK signals provides high interference immunity.

## 8. THRESHOLDING FOR SIGNAL DETECTION

As it is well known, when applying the Neumann-Pirson criterion, the threshold level  $z_{NP}$  is determined by the false alarm probability through the formula (29) only. The value of the real threshold  $z_0$  is equal to  $z_0 = z_{NP}\sigma$ .

If the random variable obeys the Raileigh distribution (20), then its mean value  $z_{mean}$  is written as [16]  $z_{mean} = \pi\sigma/2$ . Then, for decision thresholding, we get

$$z_0 = 2z_{NP}z_{mean}/\pi \quad (31)$$

where the value of  $z_{mean}$  is measured by the threshold former at the  $SUM_m$  output (Figure 5), while the coefficient  $\alpha$  (12) is equal to

$$\alpha = 2z_{NP}/\pi \quad (32)$$

For example, under the false alarm probability  $P_F = 10^{-3}$ , we obtain  $z_{NP} = 3.72$  from Equation (29), and  $\alpha = 2.37$  from Equation (32). Taking into account the increase of the interference level at the moment when signal appears, the value of  $\alpha$  should be increased by 1.5-2 times.

## 9. HARDWARE IMPLEMENTATION OPTIONS

In order to implement the proposed algorithm for detecting the PSK signal, the FPGAs, in particular, the ones of the Spartan-6 family (for example, XC6SL25) developed by Xilinx can be efficiently used [12, 13]. Simulation in the ISE WebPACK environment demonstrates that the FPGA hardware resources are sufficient for implementing the detector presented in Figure 2 under the value of  $N$  lying within the range between 16 to 2048 (in case when the value of  $n$ , the signal accumulation steps, is up to 11). The operating frequencies are determined by both the acceptable clock frequency of the ADC and the operating speed of the FPGA. In the considered example, the signal is processed at the frequencies up to 20-40 MHz and under the power consumption not exceeding 100 mW.

## 10. CONCLUSION

The introduced digital algorithm for detecting the binary phase-shift keyed signal provides its detection with high interference immunity while the signal-to-noise ratio may be considerable lower than the working value in the information receiver path. This algorithm requires a small number of arithmetic operations to be fulfilled, and it can be relatively simply implemented on the basis of the modern programmable logic devices. The detection efficiency increases with the number of the periods for averaging; but, however, in this case, the detector lag also rises. Estimating the interference level at the output of the reception path allows a relatively inexpensive implementation of the adaptive choice of the threshold for the decision concerning the presence or the absence of the signal.

## 11. ACKNOWLEDGEMENT

This research was financially supported by the Russian Foundation for Basic Research (research project no. 16-01-00121) and the Ministry of Education and Science of the Russian Federation (research project no. 2.3208.2017/4.6).

## 12. REFERENCES

- Gholami, M., and Ardeshtir, G., "Dual phase detector based on delay locked loop for high speed applications", *International Journal of Engineering, Transactions A: Basics*, Vol. 27, No. 4, (2014), 517-522.
- Gholami, M. "Phase frequency detector using transmission gates for high speed applications", *International Journal of Engineering, Transactions A: Basics*, Vol. 29, No. 7, (2016), 906-910.

3. Jiang, L., Yan, S., Wu, Y., and Ma, X., "Sonar Detection Performance with LFM-BPSK Combined Waveforms", OCEANS 2016 – Shanghai, Shanghai, China, (2016).
4. Chesi, G., Olivares, S., Paris, M.G.A., "Squeezing-enhanced phase-shift-keyed binary communication in noisy channels", *Physical Review A*, Vol. 97, No. 3, (2018), 032315.
5. Sklar, B., "Digital Communications: Fundamentals and Applications", New Jersey, Prentice Hall, (2001).
6. Proakis, J., and Salehi, M., "Digital Communications", New York, McGraw-Hill, (2007).
7. Hill, D. A., and Bodie, J. B., "Experimental carrier detection of BPSK and QPSK direct sequence spread spectrum signals", 1995 Military Communications Conference (MILCOM), San Diego, CA, USA, (1995).
8. Hill, D. A., and Bodie, J. B., "Carrier detection of PSK signals", *IEEE Transactions on Communications*, Vol. 49, No. 3, (2001), 487-496.
9. Litvinenko, V. P., Litvinenko, Yu. V., Matveev, B. V., Chernoyarov, O. V., and Makarov, A. A., "The New Detection Technique of Phase-Shift Keyed Signals", 2016 International Conference on Applied Mathematics, Simulation and Modelling (AMSM2016), Beijing, China, (2016).
10. Glushkov, A.N., Litvinenko, V. P., Litvinenko, Yu. V., Matveev, B. V., Chernoyarov, O. V., and Salnikova, A.V., "Basic Algorithm for the Coherent Digital Processing of the Radio Signals", 2015 International Conference on Space Science and Communication (IconSpace), Langkawi, Malaysia, (2015).
11. Chernoyarov, O.V., Glushkov, A.N., Litvinenko, V.P., Livinenko, Yu.V., and Matveev, B.V., "Fast Digital Algorithms for the Coherent Demodulation of the Phase-Shift Keyed Signals", 2017 IEEE Dynamics of Systems, Mechanisms and Machines (Dynamics), Omsk, Russia, (2017).
12. Maxfield, C., "The Design Warrior's Guide to FPGAs: Devices, Tools and Flows", New Jersey, Newnes, (2004).
13. Zivarian, H., Soleimani, M., and Doost Mohammadi, M.H., "Field programmable gate array-based implementation of an improved algorithm for objects distance measurement", *International Journal of Engineering, Transactions A: Basics*, Vol. 30, No. 1, (2017), 57-65.
14. Wesołowski, K., "Introduction to Digital Communication Systems", Delhi, Wiley, (2009).
15. Rabiner, L. R., and Gold, B., "Theory and Application of Digital Signal Processing", New Jersey, Prentice Hall, (1975).
16. Levin, B. R., "Theoretical Principles of Radioengineering Statistics", Virginia, Defense Technical Information Center, (1968).

## Digital Binary Phase-shift Keyed Signal Detector

O. V. Chernoyarov<sup>a,b,c</sup>, L. A. Golpaiegani<sup>c</sup>, A. N. Glushkov<sup>d</sup>, V. P. Litvinenko<sup>e</sup>, B. V. Matveev<sup>e</sup>

<sup>a</sup> International Laboratory of Statistics of Stochastic Processes and Quantitative Finance, National Research Tomsk State University, Tomsk, Russia

<sup>b</sup> Department of Higher Mathematics and System Analysis, Maikop State Technological University, Maikop, Russia

<sup>c</sup> Department of Electronics and Nanoelectronics, National Research University "MPEI", Moscow, Russia

<sup>d</sup> Department of Infocommunication Systems and Technologies, Voronezh Institute of the Ministry of Internal Affairs of the Russian Federation, Voronezh, Russia

<sup>e</sup> Department of Radio Engineering, Voronezh State Technical University, Voronezh, Russia

### P A P E R I N F O

### چکیده

#### Paper history:

Received 26 September 2018

Received in revised form 17 February 2019

Accepted 07 March 2019

#### Keywords:

Phase-shift Keying

Signal Detection

Fast Digital Processing

Noise Interference

Interference Immunity

در این کار الگوریتم مؤثری برای آشکارسازی سیگنال های دیجیتال باینری فشرده شده توسعه داده شده است. این الگوریتم نیاز به تعداد کمی از عملیات محاسباتی در طول دوره سیگنال دارد و می تواند نسبتاً آسان بر اساس دستگاه های منطقی قابل برنامه ریزی پیاده سازی شود. همچنین با تشخیص وجود سیگنال، وقتی که نسبت سیگنال به نویز بسیار کمتر از مقدار کاری آن در مسیر دریافت است، مصونیت تداخل بالا را فراهم می کند. آشکارساز معرفی شده دارای فرکانس ذاتی انتخابی است و به ما امکان میدهد تا تخمین سطح نویز را برای رسیدن به تعریف سازگار آستانه تصمیم گیری بسازیم. به منظور تأیید کارایی و عملکرد آشکارساز، عباراتی برای آلازم اشتباه و احتمالات از دست رفته پیشنهاد شده است و از لحاظ نظری و تجربی، تأثیر پارامترهای آشکارساز بر ویژگی های آن مورد بررسی قرار گرفته است.

doi: 10.5829/ije.2019.32.04a.08